Trace Analysis by SEM/EDS

© Springer Science+Business Media LLC 2018
J. Goldstein et al., *Scanning Electron Microscopy and X-Ray Microanalysis*,
https://doi.org/10.1007/978-1-4939-6676-9_21

"Trace analysis" refers to the measurement of constituents presents at low fractional levels. For SEM/EDS the following arbitrary but practical definitions have been chosen to designate various constituent classes according to these mass concentration (C) ranges:

Major: $C > 0.1$ mass fraction (greater than 10 wt%)
Minor: $0.01 \leq C \leq 0.1$ (1 wt% to 10 wt%)
Trace: $C < 0.01$ (below 1 wt%)

Note that by these definitions, while "major" and "minor" constituents have defined ranges, "trace" has no minimum. Strictly, the presence of a single atom of the element of interest within the electron-excited mass that is analyzed by X-ray spectrometry represents the ultimate trace level that might be measured for that species, but such detection is far below the practical limit for electron-excited energy dispersive X-ray spectrometry of bulk specimens. In this section trace analysis down to levels approaching a mass fraction of $C = 0.0001$ (100 ppm (ppm) will be demonstrated. While such trace measurements are possible with high count EDS spectra, achieving reliable trace measurements by electron-excited energy dispersive X-ray spectrometry requires careful attention to identifying and eliminating, if possible, pathological contributions to the measured spectrum from unexpected remote radiation sources such as secondary fluorescence and backscattered electrons (Newbury and Ritchie 2016).

21.1 Limits of Detection for SEM/EDS Microanalysis

How does the measured EDS X-ray intensity (counts in the energy window) for an element behave for constituents in the trace regime? As described in the modules on X-ray physics and on quantitative X-ray microanalysis, the X-ray spectrum that is measured is a result of the complex physics of electron-excited X-ray generation and of subsequent propagation of X-rays through the specimen to reach the EDS spectrometer. The intensity measured for the characteristic X-rays of a particular element in the excited volume is affected by all other elements present, creating the so-called matrix effects: (1) the atomic number effect that depends on the rate of electron energy loss and on the number of backscattered electrons and the BSE energy distribution; (2) the absorption effect, where the mass absorption coefficient depends on all elements present; and (3) the secondary fluorescence effect, where the absorption of characteristic and continuum X-rays with photon energies above the ionization energy of the element of interest leads to additional emission for that element. Consider the number of X-rays, N_A, including characteristic plus continuum, measured in the energy window that spans the peak for element "A" as a function of the concentration C_A in a specific mixture of other elements "B," "C," "D," and so on. A simple example would be a binary alloy system where there is complete solid solubility from pure "A" to pure "B," for example, Au-Cu or Au-Ag. When element "A" is present as a major constituent, as the concentration of "A" is reduced and replaced by "B," the matrix effects are likely to change significantly as the composition is changed. The impact of "B" on electron scattering and X-ray absorption of "A" is likely to produce a complex and non-linear response for N_A as a function of C_A. However, when the element of interest "A" is present in the trace concentration range, the matrix composition is very nearly constant as the concentration of "A" is lowered and replaced by "B," resulting in a monotonic dependence for N_A as a function of C_A, as shown in Fig. 21.1, known as a "working curve," which in the case of a dilute constituent will be linear. Consider that we have a known point on this linear plot with the values (N_s, C_s) in the trace concentration range that corresponds to the measurement of a known standard or is the result of a quantitative analysis of an unknown. The slope m of this linear function can be calculated from this known point and the 0 concentration point, for which $N_A = 0 + N_{cm}$, since there will still be counts, N_{cm}, in the "A" energy window due to the X-ray continuum produced by the other element(s) that comprise the specimen:

$$\text{slope} = \left(N_s - N_{cm}\right) / \left(C_s - 0\right) \tag{21.1}$$

The slope-intercept form ($y = mx + b$) for the linear expression for the X-ray counts in the "A" energy window, N_A, as a function of concentration, C_A, can then be constructed as:

$$N_A = \left[\left(N_s - N_{cm}\right) / \left(C_s - 0\right)\right] C_A + N_{cm} \tag{21.2}$$

The y-axis intercept, b, is equal to N_{cm}, as shown in Fig. 21.1. Because of the presence of the continuum background at all

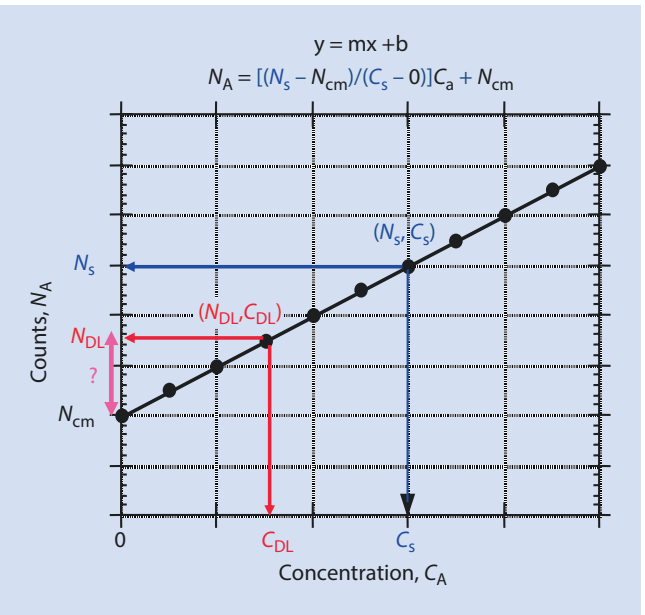

Fig. 21.1 Linear working curve for a constituent at low concentration in an effectively constant matrix

photon energies, the concentration limit of detection, C_{DL}, must have a finite, non-zero value that will be found at some point (N_{DL}, C_{DL}) along the linear response between (N_{cm}, 0) and (N_s, C_s). The work of (Currie 1968) can be used to define the condition at which the counts from the characteristic X-ray emission can be distinguished with a high degree of confidence above the natural statistical fluctuations in the background counts: the characteristic counts must exceed three times the standard deviation of the background:

$$N_A > 3N_{cm}^{1/2} \quad (21.3)$$

Thus, at the concentration limit of detection, C_{DL}:

$$N_{DL} = \text{continuum} + \text{characteristic} = N_{cm} + 3N_{cm}^{1/2} \quad (21.4a)$$

$$N_{DL} - N_{cm} = 3N_{cm}^{1/2} \quad (21.4b)$$

Substituting these conditions for (N_{DL}, C_{DL}) in Eq. (21.2):

$$N_{DL} = \left[\left(N_s - N_{cm}\right)/\left(C_s - 0\right)\right]C_{DL} + N_{cm} \quad (21.5a)$$

$$N_{DL} - N_{cm} = 3N_{cm}^{1/2} = \left[\left(N_s - N_{cm}\right)/\left(C_s - 0\right)\right]C_{DL} \quad (21.5b)$$

$$C_{DL} = \left[3N_{cm}^{1/2}/\left(N_s - N_{cm}\right)\right]C_s \quad (21.5c)$$

Equation (21.5c) enables estimation of C_{DL} from the results of a single analysis of an unknown or from a single measurement of a known standard to provide a value for C_s. The corresponding measured EDS spectrum is used to determine N_s and N_{cm}. If n repeated measurements are made, N_s and N_{cm} are then taken as averages, $\dot{N}_s$ and $\dot{N}_{cm}$, over the n measurements, and Eq. (21.5c) becomes

$$C_{DL} = \left[3\dot{N}_{cm}^{1/2}/\left(\dot{N}_s - \dot{N}_{cm}\right)n^{1/2}\right]C_s \quad (21.6)$$

C_{DL} is an estimate of the concentration level of a constituent that can just be detected with a high degree of confidence. Quantification at C_{DL} is not reasonable because the error budget is dominated by the variance of the continuum. To achieve meaningful quantitation of trace constituents, (Currie 1968) further defines a minimum quantifiable concentration, C_{MQ}, which requires that the characteristic intensity exceed $10\,\dot{N}_{cm}^{1/2}$: Inserting this criterion in Eq. 21.5c gives

$$C_{MQ} = \left[10N_{cm}^{1/2}/\left(N_s - N_{cm}\right)\right]C_s \quad (21.7)$$

21.2 Estimating the Concentration Limit of Detection, C_{DL}

Equation (21.5c) or (21.6), as appropriate to single or multiple repeated measurements, can be used to estimate the concentration limit of detection for various situations.

21.2.1 Estimating C_{DL} from a Trace or Minor Constituent from Measuring a Known Standard

Figure 21.2 shows a high count silicon drift detector (SDD)-EDS spectrum of K493 (and the residual spectrum after fitting for O, Si, and Pb), in NIST Research Material glass with the composition (as-synthesized) listed in Table 21.1. Table 21.1 also lists the measured peak intensity N_s and the background N_{cm} determined for this spectrum with the EDS spectrum measurement tools in DTSA-II. For a single measurement, the values for C_s, N_s, and N_{cm} inserted in Eq. (21.5c) gives the estimate of C_{DL} for each trace element, as also listed in Table 21.1. If $n = 4$ repeated measurements were made (or a single measurement was performed at four times the dose), C_{DL} would be lowered by a factor of 2. Examination of the values for C_{DL} in Table 21.1 reveals more than an order-of-magnitude variation depending on atomic number, for example, $C_{DL} = 52$ ppm for Al while $C_{DL} = 754$ ppm for Ta. This strong variation arises from differences in the relative excitation (overvoltage) and fluorescence yield for the various elements, differences in the continuum intensity, and the partitioning of the characteristic X-ray intensity among widely separated peaks for the L-family of the higher atomic number elements, for example, Ce and Ta.

21.2.2 Estimating C_{DL} After Determination of a Minor or Trace Constituent with Severe Peak Interference from a Major Constituent

Because of the relatively poor energy resolution of EDS, peak interference situations are frequently encountered. Multiple linear least squares peak fitting can separate the contributions from two or more peaks within an energy window. This effect is illustrated in Fig. 21.3 for Corning Glass A, the composition of which is listed in Table 21.2 along with the DTSA II analysis. There is a significant interference for K and Ca upon Sb and Sn. The initial qualitative analysis identified K and Ca, as shown in Fig. 21.3(a). When MLLS peak fitting is applied for K and Ca, the Sn and Sb L-family peaks are revealed in the residual spectrum, Fig. 21.3(b). The limit of detection calculated from the peak for Sn L determined from peak and background intensities determined from this residual spectrum is $C_{DL} = 0.00002$ (200 ppm).

21.2.3 Estimating C_{DL} When a Reference Value for Trace or Minor Element Is Not Available

Another type of problem that may be encountered is the situation where the analyst wishes to estimate C_{DL} for hypothetical

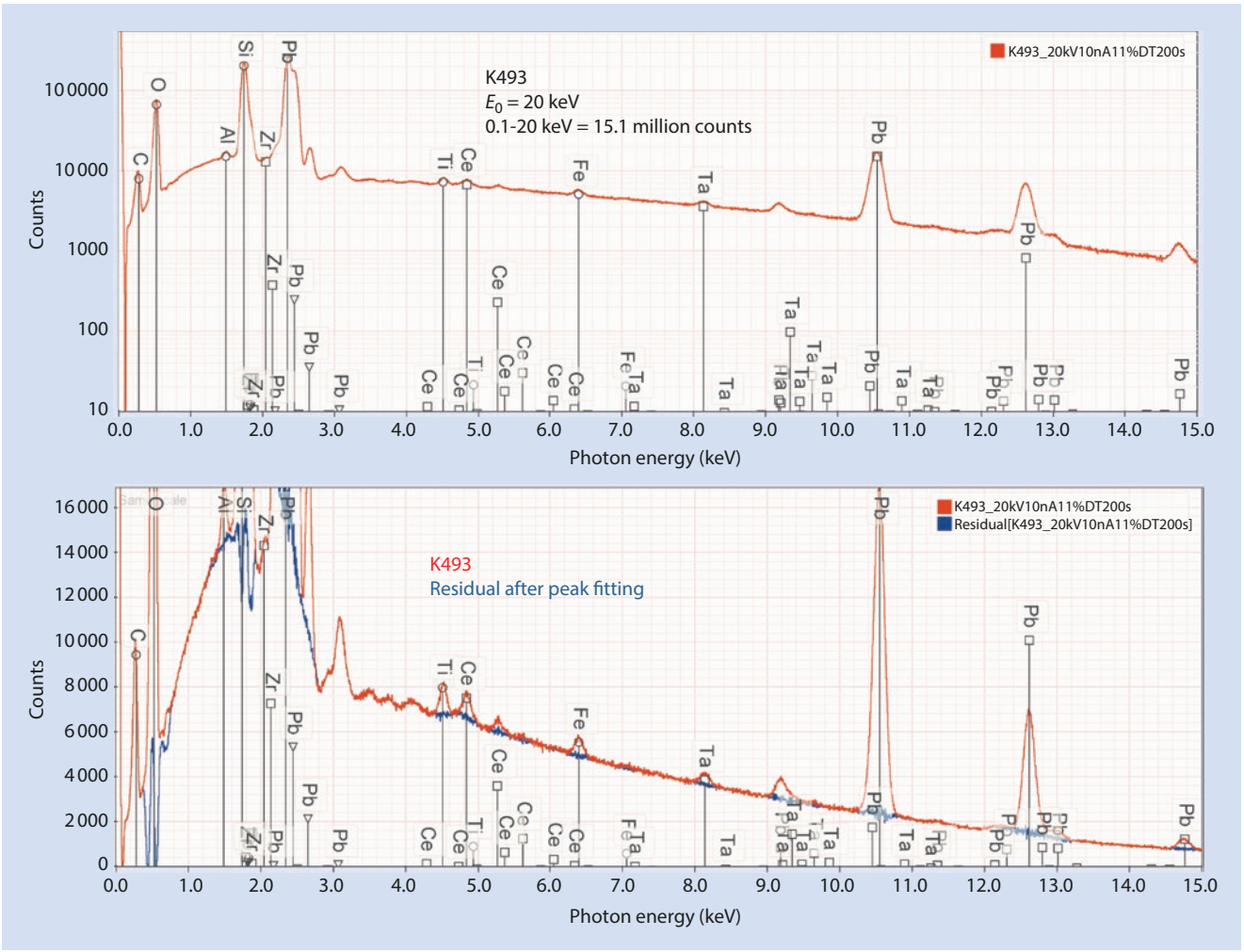

Fig. 21.2 SDD-EDS spectrum (0.1–20 keV = 29 million counts) of NIST Research Material Glass K493 at E_0 = 20 keV and residual after MLLS peak fitting for O, Si, and Pb

Table 21.1 Limits of detection estimated from a known standard K493 (E_0 = 20 keV 0.1–20 keV = 29 million counts)

Element	Mass conc	N_s (counts)	N_{cm} (counts)	C_{DL} (mass conc)	C_{DL} (ppm)
O	0.2063				
Al	0.00106	434,999	396,617	0.000052	52 ppm
Si	0.1304				
Ti	0.00192	280,709	255,991	0.000118	118 ppm
Fe	0.00224	229,356	210,799	0.000166	166 ppm
Zr	0.00363	313,728	303,760	0.000602	602 ppm
Ce (L)	0.00554	291,575	269,042	0.000383	383 ppm
Ta (L)	0.00721	156,283	145,340	0.000754	754 ppm
Pb	0.6413				

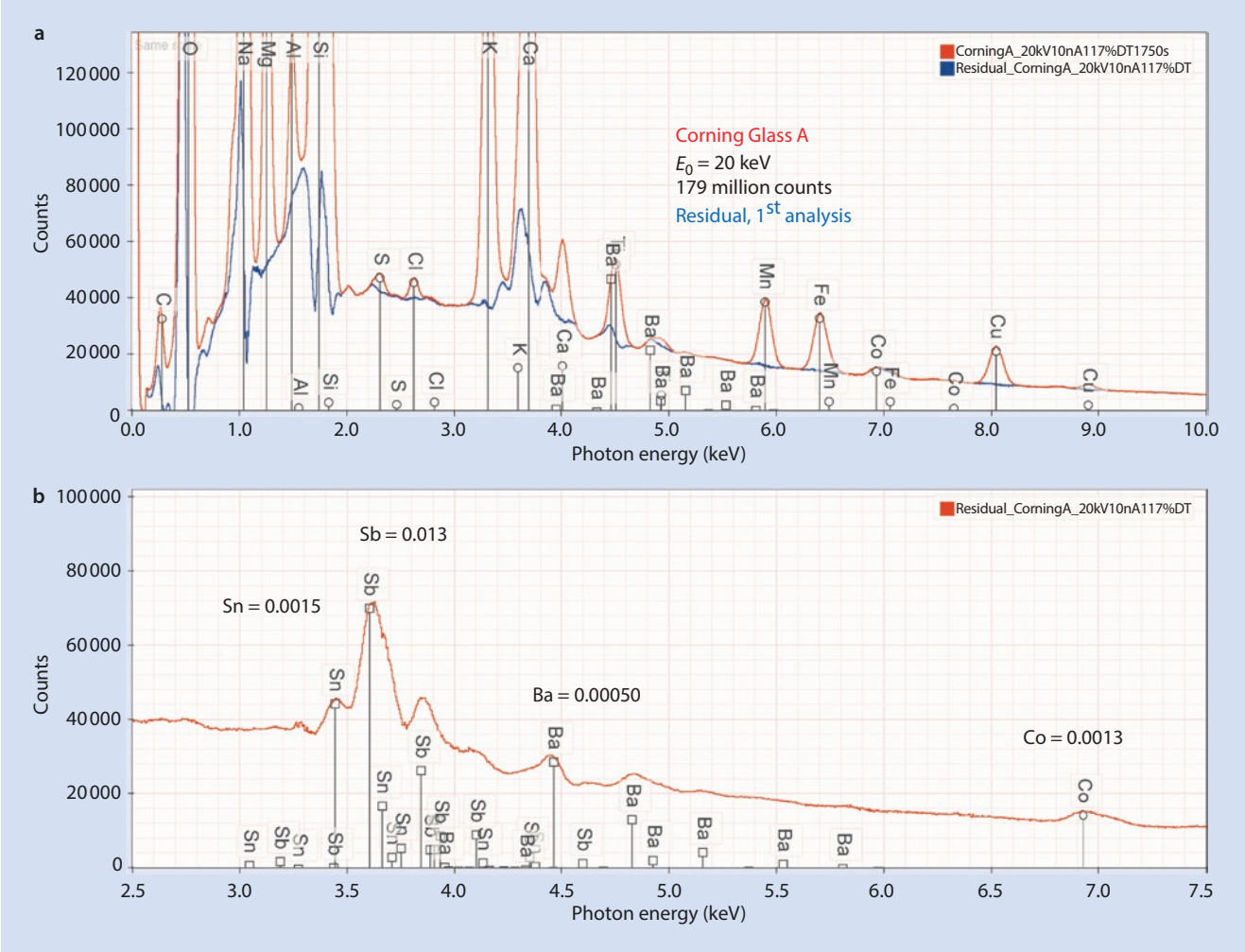

Fig. 21.3 **a** SDD-EDS spectrum (0.1–20 keV = 7.8 million counts) of Corning Glass A at $E_0 = 20$ keV and residual spectrum after MLLS peak fitting for K and Ca. **b** Expansion of K and Ca region showing detection of Sn and Sb L-family X-rays

trace constituents that might be present in regions of the spectrum that consist only of the X-ray continuum background. An example is shown in Fig. 21.4 for high purity Si. The spectrum consists of the Si K-shell X-rays, the associated coincidence peak, and the X-ray continuum background. Consider that the task is to estimate C_{DL} for several elements, for example, Al, Cr, and Cu. In the absence of a specimen of Si with known trace or minor levels of these elements, a reasonable estimate of C_{DL} can be made by determining the threshold k-ratio relative to a pure element, as illustrated for Cr and Cu with the spectra superimposed in Fig. 21.4(b). Using the energy window for Cr K-$L_{2,3}$ (CrKα), the continuum intensity in the Si spectrum at Cr K-$L_{2,3}$ is measured, $N_{cm\_Si\text{-}at\text{-}Cr}$, and is divided by the Cr K-$L_{2,3}$ intensity from the Cr spectrum at the equivalent dose, giving the k-ratio k_{DL} for detection:

$$k_{DL} = 3\, N^{½}_{cm\_Si\text{-}at\text{-}Cr} / N_{Cr} \qquad (21.8)$$

Values of for k_{DL} for Al, Cr, and Cu as measured for this Si spectrum are listed in Table 21.3. These k-ratios can be converted into CDL values by calculating the ZAF matrix correction factors for these constituents at trace levels in Si with DTSA-II, although this is generally a small correction.

21.3 Measurements of Trace Constituents by Electron-Excited Energy Dispersive X-ray Spectrometry

21.3.1 Is a Given Trace Level Measurement Actually Valid?

Trace analysis with high count EDS spectra can be performed to concentrations levels down to 0.0001 mass fraction (100 ppm) in the absence of interferences and 0.0005 (500 ppm) when peak interference occurs. The careful analyst will always ask the question, Is a given trace measurement valid? That is, does the measured trace constituent actually originate within the interaction volume of the specimen that is excited by primary electron beam, or is it the result of remote excitation of another part of the specimen or from components of the SEM itself?

Table 21.2 Corning Glass A, as synthesized and as analyzed with DTSA-II ($E_0 = 20$ keV) [O by stoichiometry; Na (albite); Ca, P (fluoroapatite); S (pyrite); K, Cl (KCl); Sr ($SrTiO_3$); Ba aSi_2O_5); Pb (PbTe); Mg, Al, Si, Ti, Mn, Fe, Co, Cu, Zn, Sn, Sb (pure elements)]

Element	As-synthesized (mass conc)	DTSA-II analysis (mass conc)
O	0.4407	0.4474 (stoich.)
Na	0.106	0.106 ± 0.0002
Mg	0.0160	0.0163 ± 0.0001
Al	0.0053	0.0051 ± 0.00005
Si	0.3112	0.3171 ± 0.0002
P	0.00057	0.0003 ± 0.0001
S	0.0004	0.00085 ± 0.0001
Cl	0.00069	0.00072 ± 0.00005
K	0.0238	0.0237 ± 0.0001
Ca	0.0360	0.0341 ± 0.0001
Ti	0.00474	0.00485 ± 0.0001
Mn	0.00774	0.00768 ± 0.0001
Fe	0.00762	0.00717 ± 0.0001
Co	0.00134	0.00140 ± 0.0001
Cu	0.00935	0.00933 ± 0.0001
Zn	0.00035	0.00047 ± 0.0001
Sr	0.00085	0.0156 ± 0.0006
Sn	0.0015	0.0011 ± 0.0003
Sb	0.0132	0.0128 ± 0.0002
Ba	0.00502	0.00405 ± 0.0002
Pb	0.00111	0.050 ± 0.0001

The Inevitable Physics of Remote Excitation Within the Specimen: Secondary Fluorescence Beyond the Electron Interaction Volume

The electron interaction volume contains the region within which characteristic and continuum X-rays are directly excited by the beam electrons. Electron excitation effectively creates a volume source of generated X-rays (characteristic and continuum with energies up to the incident beam energy, E_0) embedded in the specimen that propagates out from the interaction volume in all directions. A photon propagating into the specimen will eventually undergo photoelectric absorption which ionizes the absorbing atom, and the subsequent de-excitation of this atom will result in emission of its characteristic X-rays, a process referred to as "secondary fluorescence" to distinguish this source from the "primary fluorescence" induced directly by the beam electrons. Because the range of X-rays is generally one to two orders of magnitude greater than the range of electrons, depending on the photon energy and the specimen composition, the volume of secondary characteristic generation is much larger than the volume of primary characteristic generation. The range of fluorescence of Fe K-$L_{2,3}$ by Ni K-$L_{2,3}$ in a 75wt% Ni-25wt% Fe alloy at $E_0 = 25$ keV is shown in Fig. 21.5. The electron range is fully contained with a hemisphere of radius 2.5 μm, but a hemisphere of 80 -μm radius is required to capture 99 % of the secondary fluorescence of Fe K-$L_{2,3}$ by Ni K-$L_{2,3}$. For quantification with the ZAF matrix correction protocol, the secondary fluorescence correction factor, F, corrects the calculated composition for the additional radiation created by secondary fluorescence due to characteristic X-rays. An additional correction, c, is necessary for the continuum-induced secondary fluorescence. The F matrix correction factor is generally small compared to the absorption, A, and atomic number, Z, corrections. For a major constituent, the additional radiation due to secondary fluorescence represents a small perturbation in the apparent concentration, often negligible. However, when a constituent is at the trace level in the electron interaction volume, propagation of the primary characteristic and continuum X-rays into a nearby region of the specimen that is richer in this element will create additional X-rays of the trace element by secondary fluorescence. Because of the wide acceptance area of the EDS, this additional remote source of radiation will still be considered to be part of the spectrum produced at the beam position, possibly severely perturbing the accuracy of the analysis of the trace constituent by elevating the measured concentration above the true concentration. Compensation for this artifact requires careful modeling of the electron and X-ray interactions.

Simulation of Long-Range Secondary X-ray Fluorescence

The Monte Carlo electron trajectory simulation embedded in DTSA-II models the primary electron trajectories and primary X-ray generation, as well as the subsequent propagation of the primary characteristic and continuum X-rays through the target and the generation (and subsequent propagation) of secondary characteristic X-rays. The Monte Carlo menu provides "set-pieces" of analytical interest to predict the significance of secondary fluorescence at the trace level:

NIST DTSA II Simulation: Vertical Interface Between Two Regions of Different Composition in a Flat Bulk Target

Figure 21.6 shows the simulation of an interface between Cu and NIST SRM470 (K-412 glass) for a beam with an incident energy of 25 keV placed 10 μm from the interface in the Cu region. The map of the distribution of excitation reveals the propagation of X-rays from the original electron

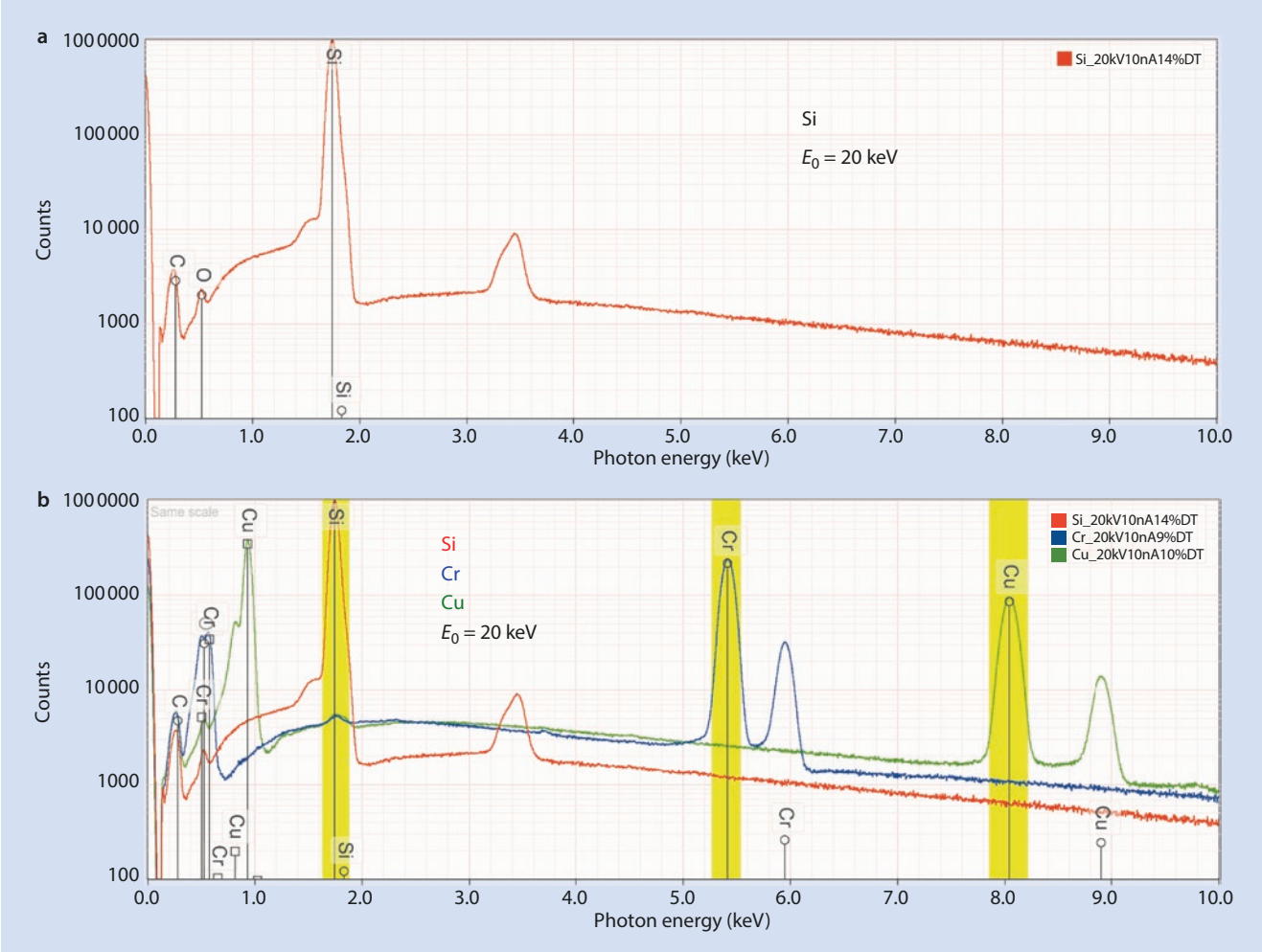

Fig. 21.4 **a** SDD-EDS spectrum of Si (20 keV; 1000 nA-s; 0.1–20 keV = 22 million counts) with energy windows defined for Al, Cr, and Cu. **b** Spectrum for Si with the spectra of Cr and Cu superimposed

Table 21.3 Estimated limits of detection k_{DL} for a Si spectrum with 110 million counts (0.1–20 keV)

Element	k_{DL}	ZAF	C_{DL} (mass conc)	C_{DL} (ppm)
Al	0.000115	1.12	0.000129	129
Cr	0.000133	1.01	0.000134	134
Cu	0.000113	1.00	0.000113	113

interaction volume into the K412 glass to excite secondary fluorescence. The calculated spectrum shown in Fig. 21.6 shows the presence of an apparent trace level of Fe (and to a lesser extent, Ca, Si, Al, and Mg) in the Cu, corresponding to $k = 0.0028$ relative to a pure Fe standard. The Fe k-ratio as a function of beam position in the Cu is also shown in Fig. 21.6. Even with the beam placed in the Cu at a distance of 40 µm from the K-412, there is an apparent Fe trace level in the Cu of k = 0.0004, or about 400 ppm.

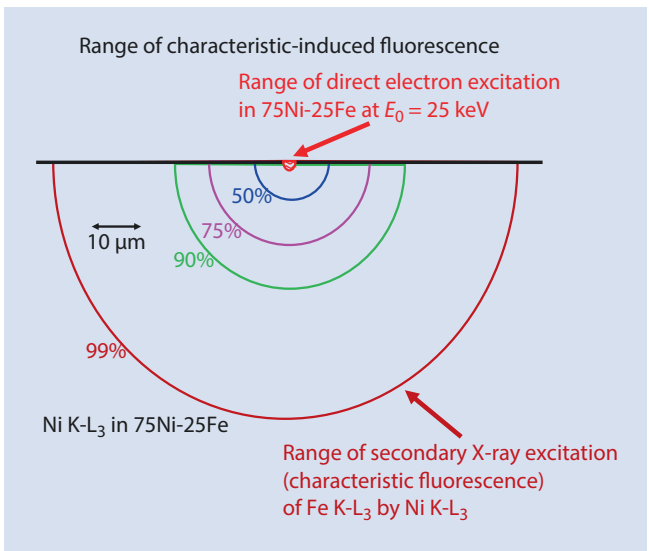

Fig. 21.5 Range of secondary fluorescence of FeKα by NiKα in a 75Ni-25Fe alloy at E_0 = 25 keV

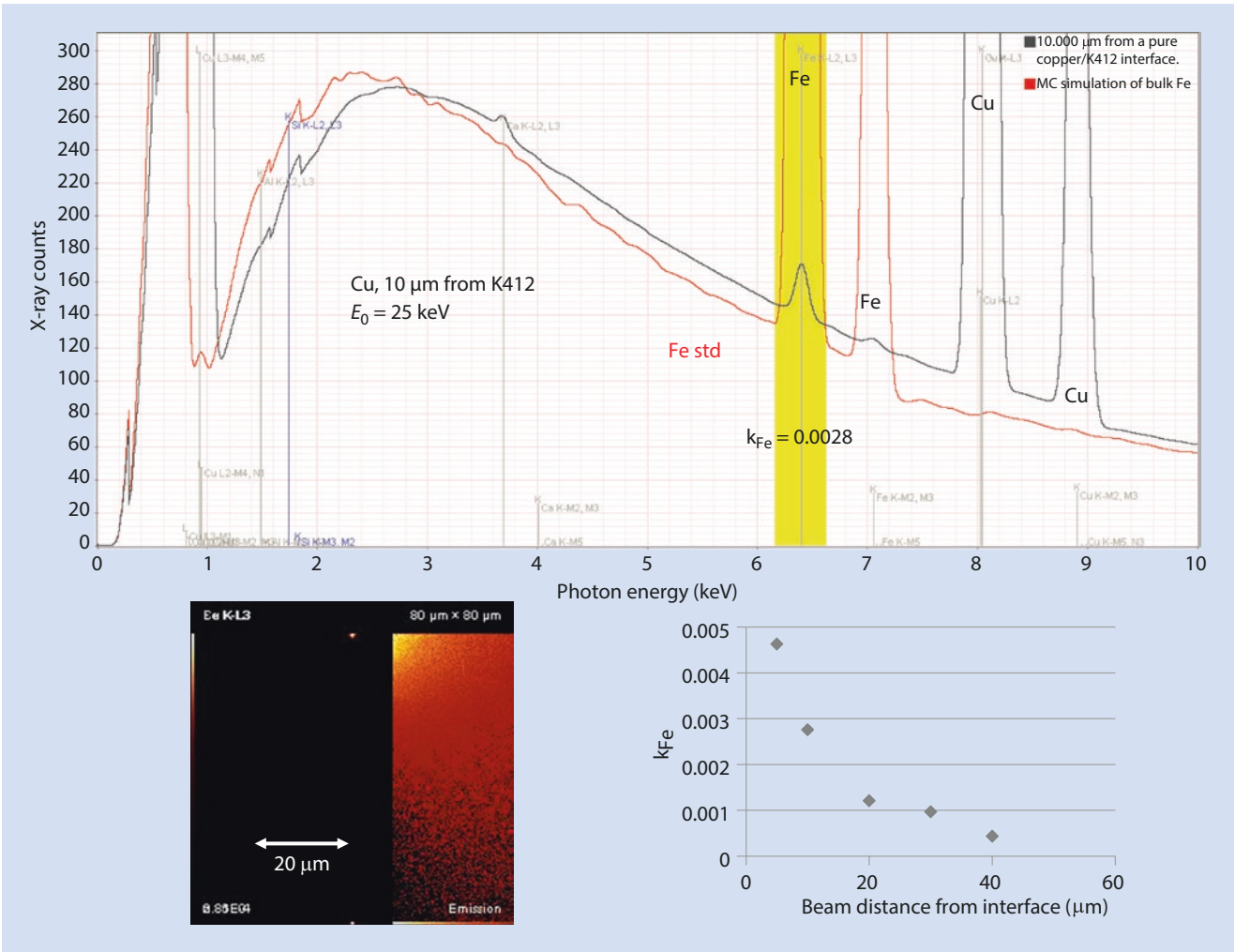

Fig. 21.6 DTSA-II Monte Carlo calculation of fluorescence across a planar boundary between copper and SRM 470 (K-412 glass). The beam is placed in the copper at various distances from the interface. The spectrum calculated for a beam at 10 µm from the interface shows a small Fe peak, which is ratioed to the intensity calculated for pure iron, giving $k_{Fe} = 0.0028$. The inset map of the distribution of secondary FeKα X-ray production shows the extent of penetration of characteristic Cu Kα and Cu Kβ and continuum X-rays into the K-412 glass to fluoresce FeKα. Simulations at other distances give the response plotted in the graph

NIST DTSA II Simulation: Cubic Particle Embedded in a Bulk Matrix

Figure 21.7(a) shows the results of a simulation of a 1-µm cube of K-411 glass embedded in a titanium matrix and excited with a beam energy of 20 keV. For this size and beam energy, the primary electron trajectories penetrate through the sides and bottom of the cube leading to direct electron excitation of the titanium matrix, which is seen as a major peak in the calculated spectrum. When the cube dimension is increased to 20 µm, the beam trajectories at $E_0 = 20$ keV are contained entirely within the K-411 cube. DTSA-II allows calculations with and without implementing the secondary fluorescence calculation. When secondary fluorescence is not implemented, the calculated spectrum Fig. 21.7(b) shows no Ti characteristic X-rays. When secondary fluorescence is included in the simulation, a small Ti peak is observed, corresponding to an artifact trace level $k = 0.0007$ (700 ppm), demonstrating the long range of the primary X-rays and the creation of a trace level artifact.

When variable pressure SEM operation is considered, the large fraction of gas-scattered electrons creates X-rays from regions up to many millimeters from the beam impact point. Depending on the surroundings, this gas scattering can greatly modify the EDS spectrum from what would originate from the region actually excited by the focused beam. Figure 21.7(c) shows this effect as simulated with DTSA II, resulting in a large peak for Ti, which is not present in the specimen but which is located in the surrounding region.

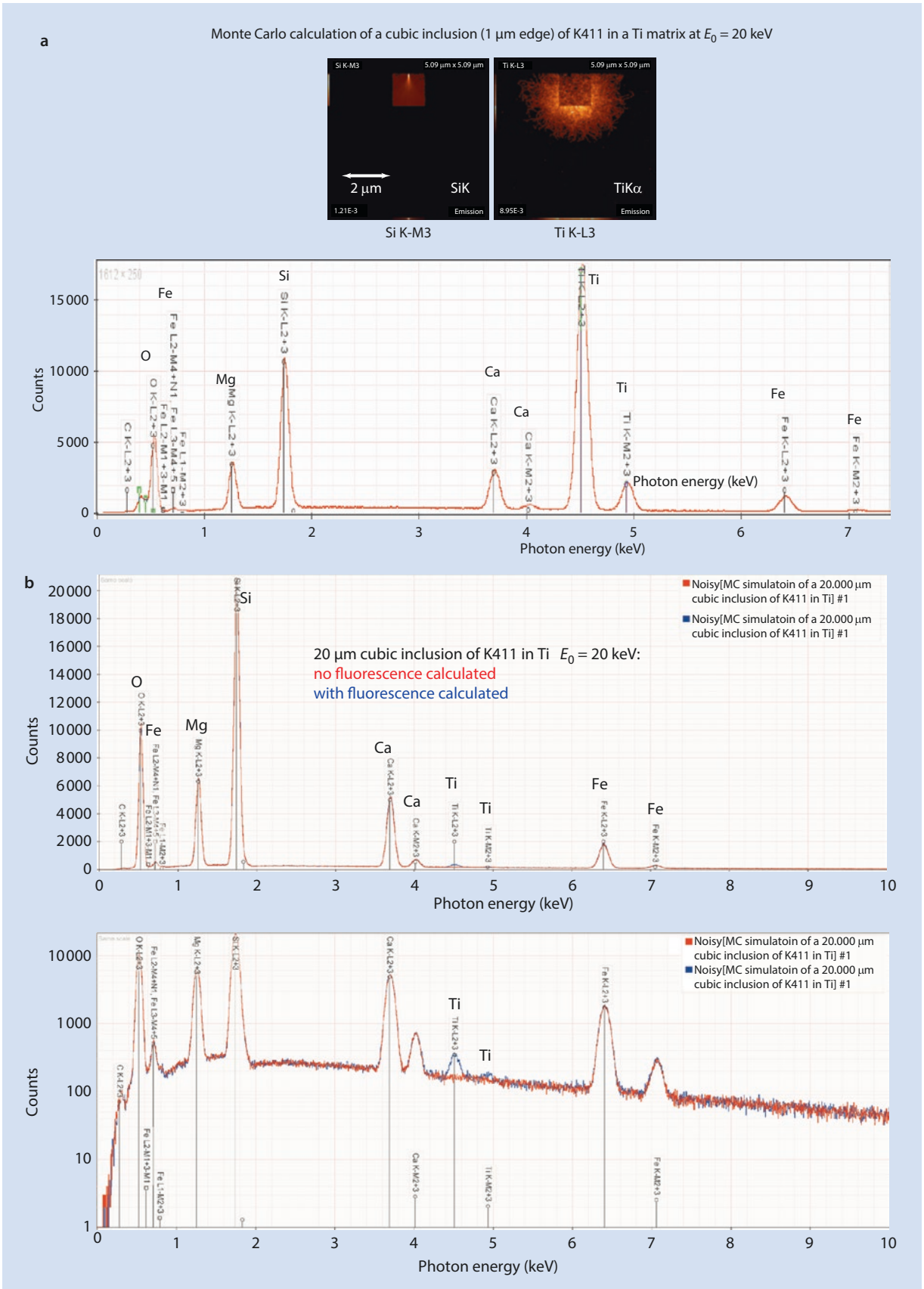

Fig. 21.7 **a** DTSA-II Monte Carlo calculation of a 1-µm cubical particle of K411 glass embedded in a Ti matrix with a beam energy of 20 keV, including maps of the distribution of SiK (particle) and TiKα (surrounding matrix). **b** 20-µm cubical particle of K411 glass embedded in a Ti with and without calculation of secondary fluorescence. **c** 20-µm cubical particle of K411 glass embedded in a Ti with calculation of secondary fluorescence and with calculation of gas scattering in VPSEM operation—water vapor; 133 Pa (1 Torr); 10-mm gas path length

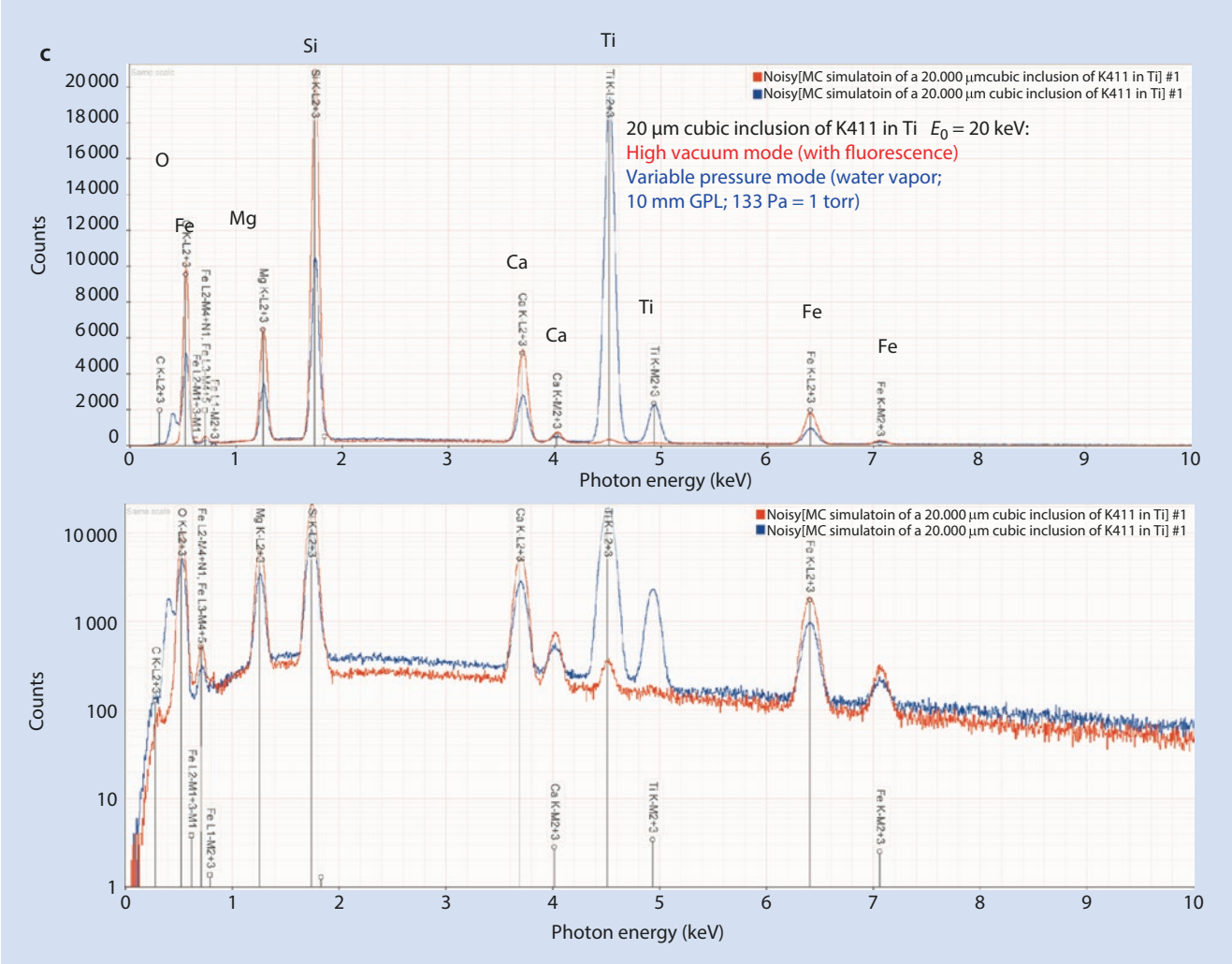

Fig. 21.7 (continued)

21.4 Pathological Electron Scattering Can Produce "Trace" Contributions to EDS Spectra

21.4.1 Instrumental Sources of Trace Analysis Artifacts

While secondary fluorescence that leads to generation of X-rays at a considerable distance from the beam impact is a physical effect which cannot be avoided, there are additional pathological scattering effects that can be minimized or even eliminated. Figure 21.8 depicts the idealized view of the emission of X-rays generated by the electron beam in the SEM. In this idealized view, the only X-rays that are collected are those emitted into the solid angle of acceptance of the detector, which is defined by a cone whose apex is centered on the specimen interaction volume, whose altitude is the specimen-to-detector distance, and whose base is the active area of the detector that is not shielded by the

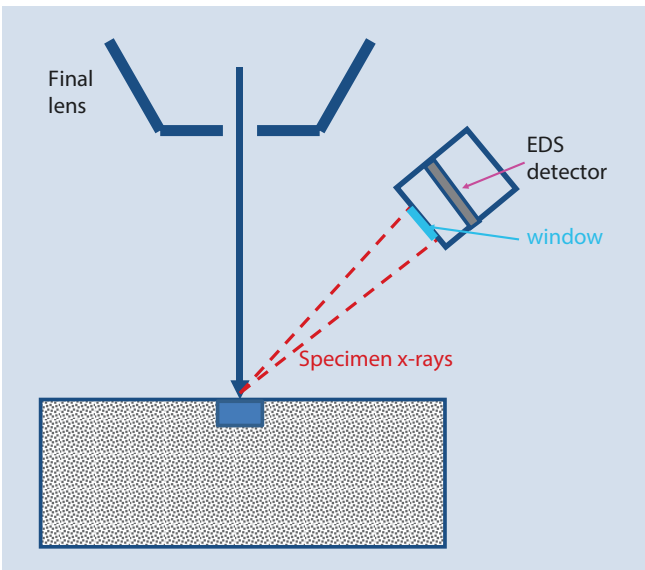

Fig. 21.8 Ideal view of the collection angle of an EDS system

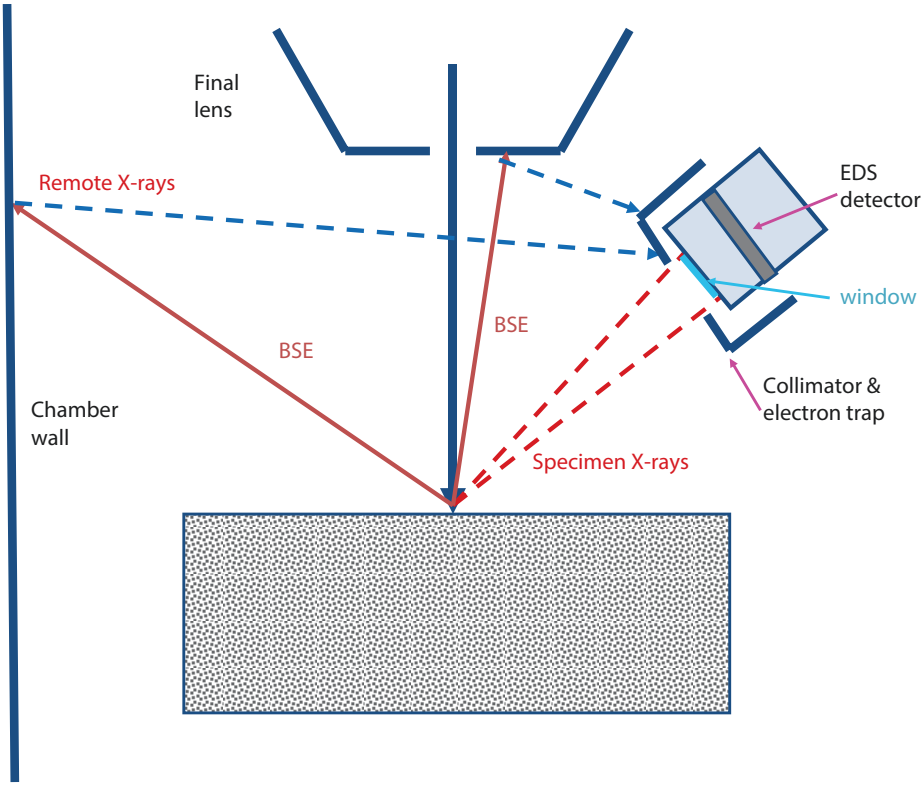

Fig. 21.9 Effect of backscattering to produce remote X-ray sources on SEM components (objective lens, chamber walls, stage, etc.) and use of collimator to block these contributions from reaching the EDS

entrance window or other hardware. However, the reality of the EDS measurement is likely to be quite different from this ideal case, at least at the trace constituent level, as a consequence of electron backscattering, shown schematically in Fig. 21.9. For targets of intermediate and high atomic number, a significant fraction of the incident beam is emitted as backscattered electrons, and the majority of these BSEs retain more than half of the incident beam energy. After leaving the specimen, these BSEs are likely to strike the objective lens and the walls of the specimen chamber as well as other hardware, where they generate the characteristic (and continuum) X-rays of those materials. The EDS detector collects X-rays from any source with a line-of-sight to the detector, so to minimize remote BSE-induced contributions to the measured spectrum, the EDS is equipped with a collimator whose function is to restrict the view of the EDS, as illustrated schematically in Fig. 21.9. The solid angle of acceptance of the EDS is substantially reduced by the collimator, minimizing remote contributions from the lens and chamber walls. While the collimator provides a critical improvement to the measured spectrum, it is important for the analyst to understand its inevitable limitations. The actual acceptance solid angle must be constructed by looking out from the detector through the aperture of the collimator, as shown in Fig. 21.10. The typical collimator accepts X-rays generated in the specimen plane within a circular area with a diameter of several millimeters, a feature that is important for X-ray mapping applications, where the beam is scanned over large lateral areas and X-rays must be accepted from any beam position within the scanned area. Moreover, the acceptance region is three dimensional with a vertical dimension of several millimeters along the beam axis. To determine the true acceptance volume of the EDS collimator, low magnification (maximum scanning area) X-ray mapping of a target such as a blank aluminum sample stub provides a direct view of the transmission of the EDS collimator as a function of x-y position and as a function of the z-position, as shown in Fig. 21.11. For this example, any X-ray generated in a large volume (at least $2.5 \times 3 \times 10$ mm) can potentially be collected by this EDS system despite the otherwise effective collimator. Three important sources of uncontrolled remote excitation within this collimator acceptance volume are shown in Fig. 21.12: (1) beam electrons scattering off the edge of the final aperture (magenta trajectory); (2) beam electrons being stopped by the final aperture and generating the characteristic and continuum X-rays of the aperture material (e.g., Pt; blue dashed trajectory); and (3) re-scattering of BSEs that have struck the final lens and return to the specimen (red trajectory). Both of these sources can create X-rays several millimeters or more from the beam impact location.

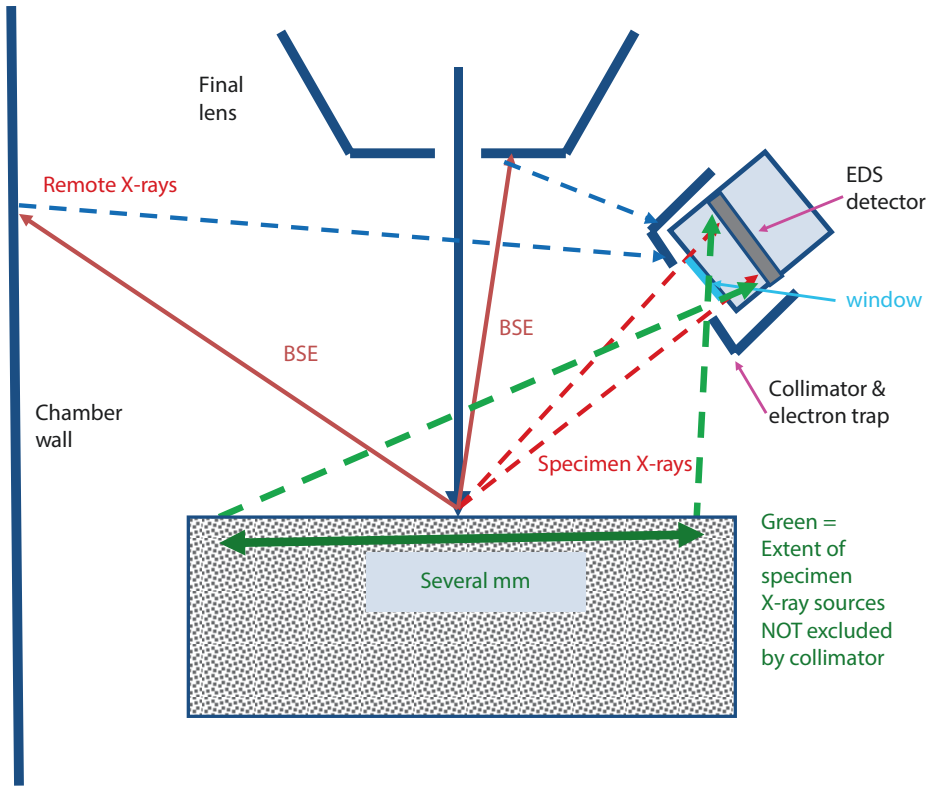

Fig. 21.10 True extent of acceptance area of EDS constructed by looking out through the collimator

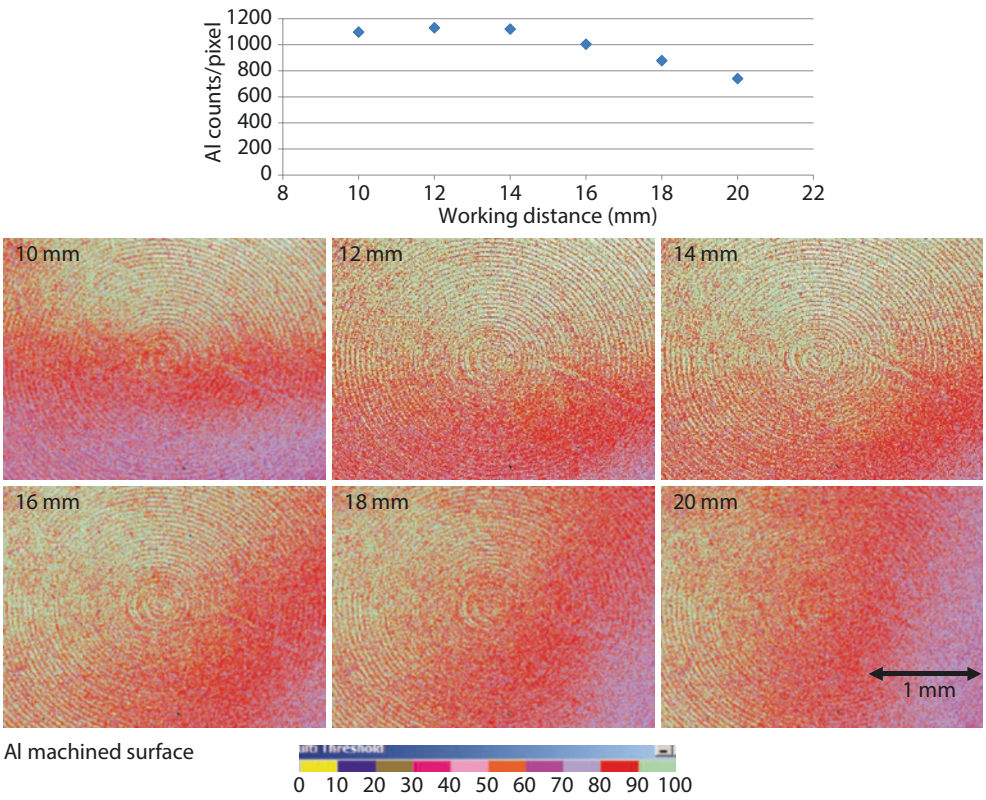

Fig. 21.11 X-ray mapping to determine the acceptance volume of the collimator. A series of Al X-ray maps of an aluminum SEM stub at different working distances is shown; the inset graph shows the intensity at the center of each map as a function of working distance

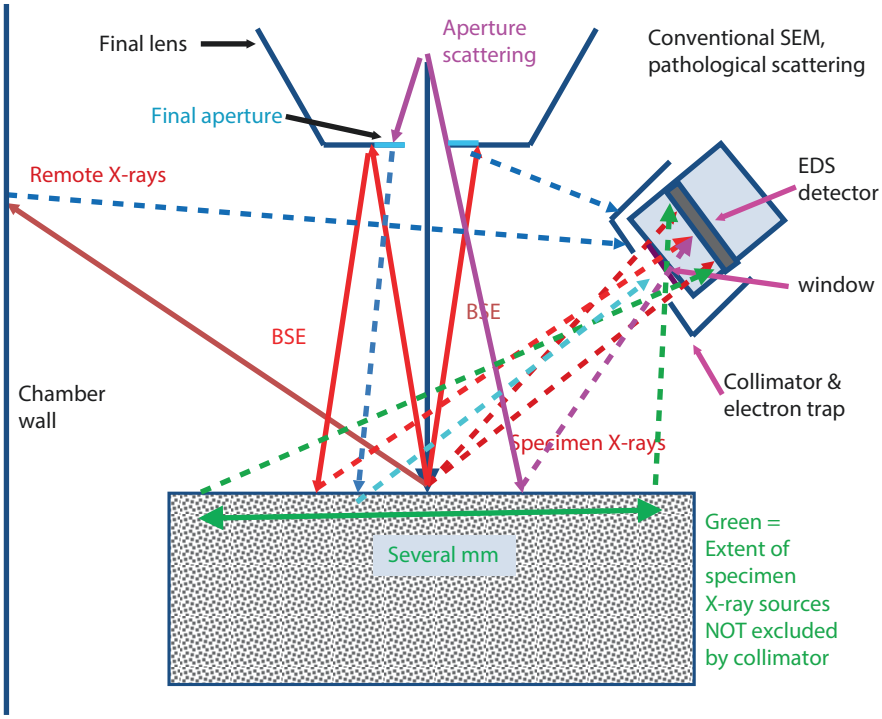

Fig. 21.12 Possible sources of remote excitation: beam electrons scattering off edge of final aperture, beams stopped by aperture generating characteristic and continuum X-rays, and re-scattering of backscattered electrons from the lens

21.4.2 Assessing Remote Excitation Sources in an SEM-EDS System

Remote excitation of X-rays can be assessed by measuring various structures. As shown in Fig. 21.13, a multi-material Faraday cup can be constructed by placing an SEM aperture (typically 2.5 mm in diameter and made of platinum or another heavy metal) over a blind hole drilled in a block of a different metal, such as a 1-cm diameter aluminum SEM stub, which is then inserted in a hole drilled in a 2.5-cm-diameter brass (Cu-Zn) block. This structure can be used to measure the "in-hole" spectrum to assess sources and magnitude of remote excitation (Williams and Goldstein 1981). The following sequence of measurements is made, as shown in Fig. 21.14. The beam is successively placed for the same dose on the brass, the Al-stub, the Pt-aperture, and finally in the center of the hole (e.g., 200-μm diameter) of the aperture. Ideally, if there are no electrons scattered outside the beam by interacting with the final aperture or other electron column surfaces, the "in-hole" specimen will have no counts. As shown in Fig. 21.14 with a logarithmic intensity display, a small number of counts is detected for Pt M, equivalent to $k = 0.00008$ of the intensity measured for the same dose with the beam placed on the Pt aperture. No detectable counts are found for Al from the stub or for the Cu and Zn from the brass block. Thus, for this particular instrument, a small but detectable pathological scattering occurs within approximately 1.5 mm of the central beam axis. While this is a very small effect, the analyst must nonetheless be aware that this unfocused electron or aperture X-ray source might contribute an artifact at the trace level if the element of interest at the beam location is abundant in a nearby region.

While a useful measurement and the place to start in assessing remote excitation, the "in-hole" measurement only detects electrons scattered outside of the beam. Typically, a more serious source of remote excitation is the backscattered electrons (BSEs), which are absent from the "in-hole" measurement. Figure 21.15 shows a modification of the "in-hole" multi-material target in which the central hole is replaced by a flat, polished scattering target. Figure 21.16 shows an example of a spectrum in which the central target is high purity carbon, which has a low BSE coefficient of 0.06, surrounded by a 3-mm-diameter region filled with Ag-epoxy, which is surrounded by a Ti block. No detectable counts for characteristic peaks of Ag (conducting epoxy) or Ti (specimen holder) are found.

Figure 21.17 shows a similar measurement for high purity tantalum, which has a high BSE coefficient of 0.45. Both Ag and Ti are detectable at very low relative intensity compared to the intensity measured with the beam placed on pure element targets.

When a three-dimensional target is used for scattering, as illustrated in Fig. 21.18, additional BSEs are scattered from the tilted surfaces into the regions of the specimen near the beam impact point as well as more distant regions surrounding the specimen. Figure 21.19 shows such a measurement for a pyramidal fragment of SrF_2 placed on a brass substrate. Low level signals are observed for CuKα and ZnKα, and also for NiKα, which arises from Ni-plating on nearby stage components. This extreme case most closely resembles the challenge posed by a rough, topographic specimen. The uncontrollable scattering renders most trace constituent determinations questionable.

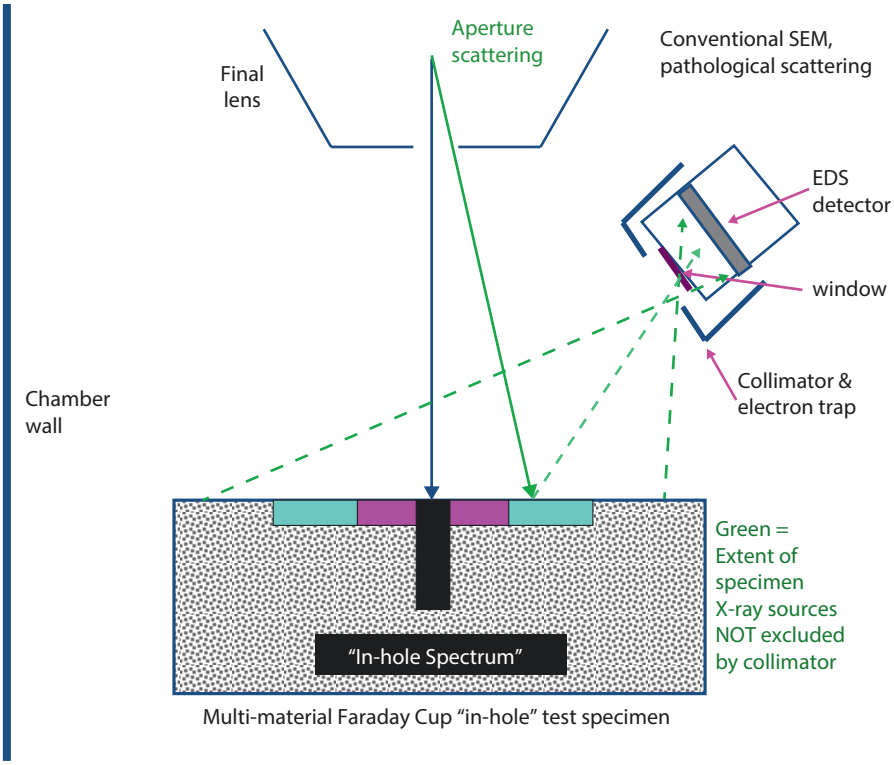

Fig. 21.13 Measurement of "in-hole" spectrum with a multi-material Faraday cup consisting of three materials arranged concentrically

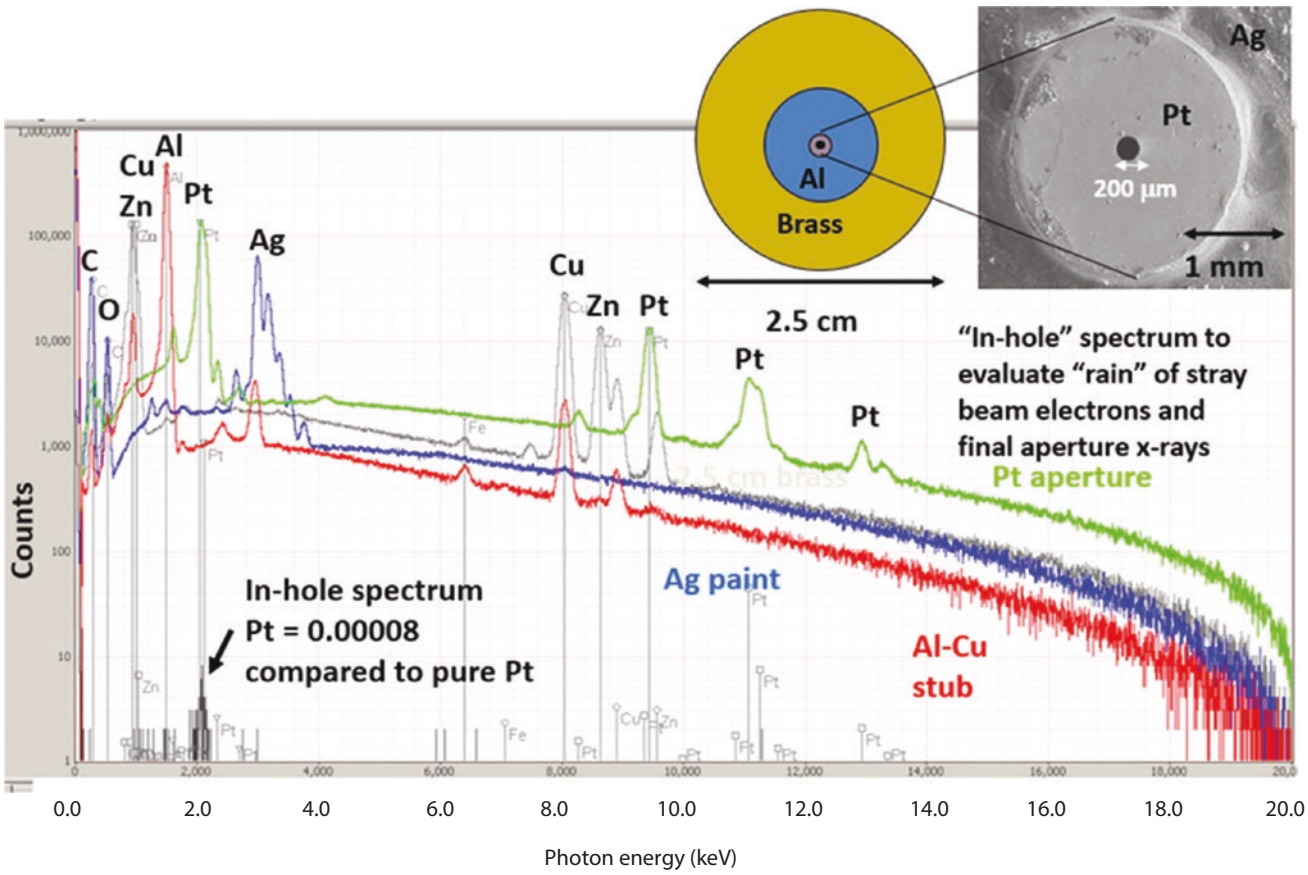

Fig. 21.14 Sequence of measurements for determining pathological scattering effects by the "in-hole" method. For the same dose, EDS spectra are measured on the brass block, aluminum stub, platinum aperture, and at the center of the 200 µm diameter hole of the platinum aperture. A logarithmic display reveals the very low counts in the "in-hole" spectrum compared to the spectra measured on the various materials

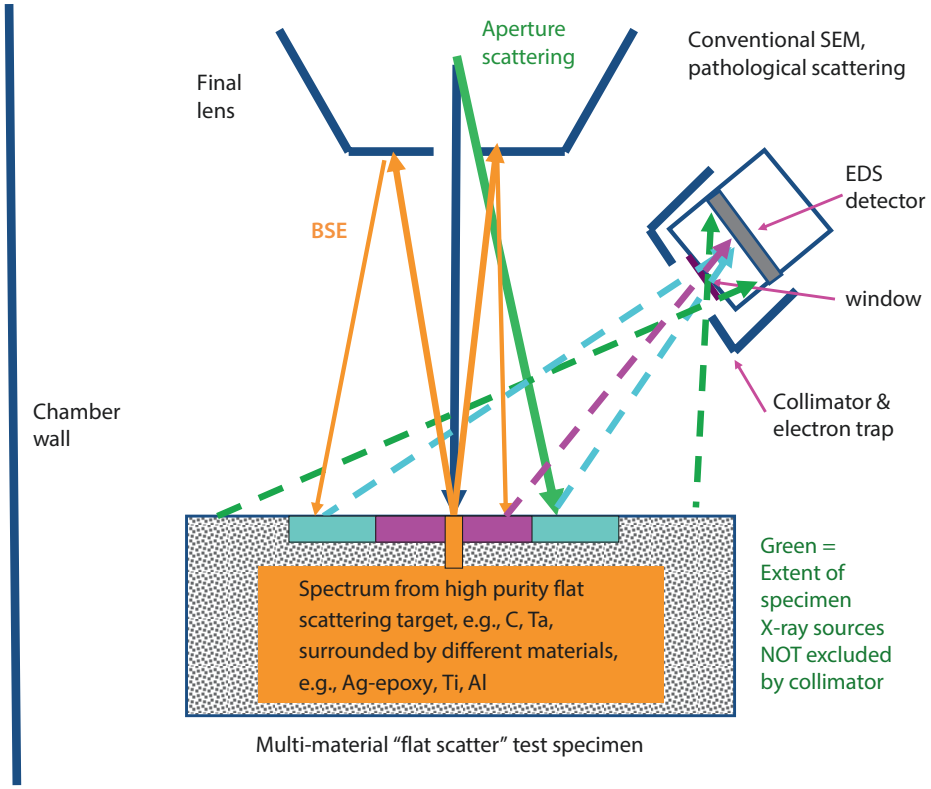

Fig. 21.15 Schematic diagram of the "in-hole" configuration with a pure element target placed at the center of a multi-material target

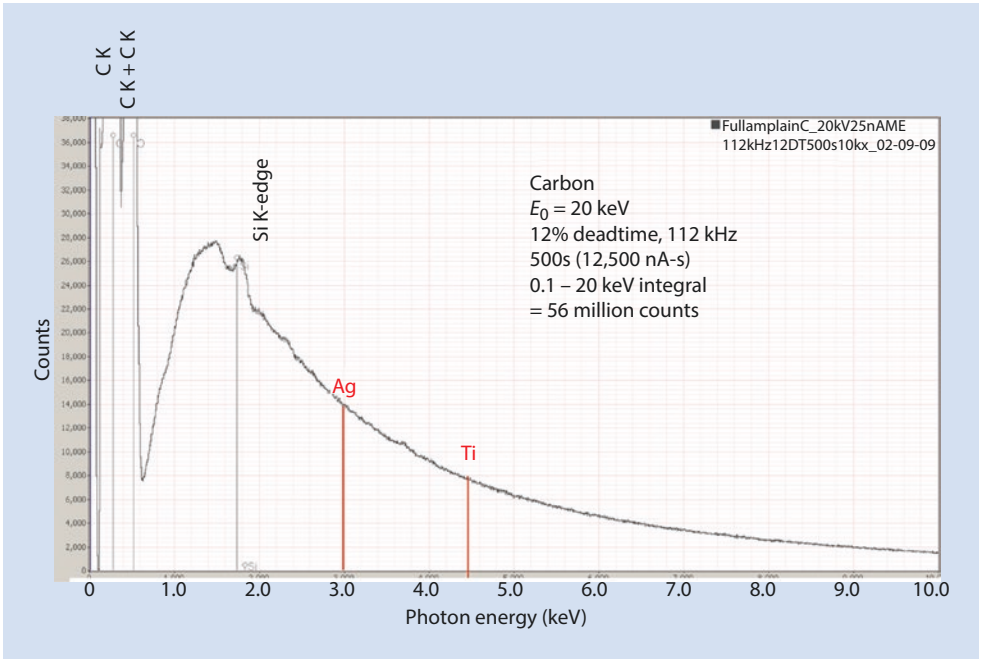

Fig. 21.16 Measurement of high purity C surrounded by Ag (doped epoxy) and titanium; no significant signals for Ag or Ti are observed

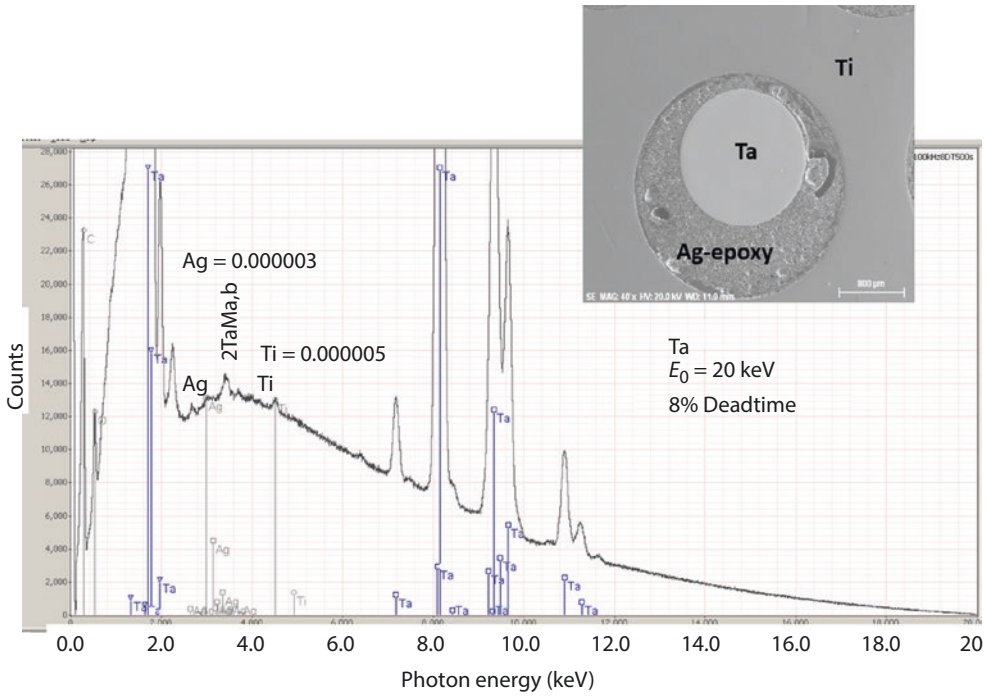

Fig. 21.17 Measurement of high purity Ta surrounded by Ag (doped epoxy) and titanium; Ag or Ti are both observed at very low levels: Ag, k = 0.000003; Ti, k = 0.000005

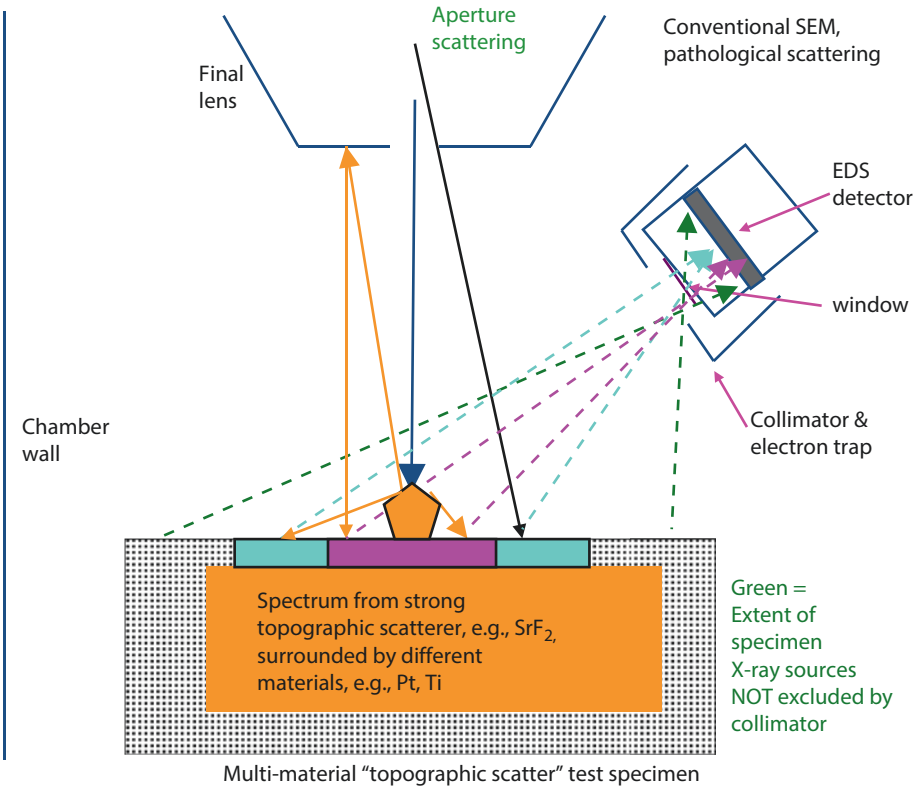

Fig. 21.18 Modification of the "in-hole" configuration with a three-dimensional target to produce the effects of backscattering from inclined surfaces

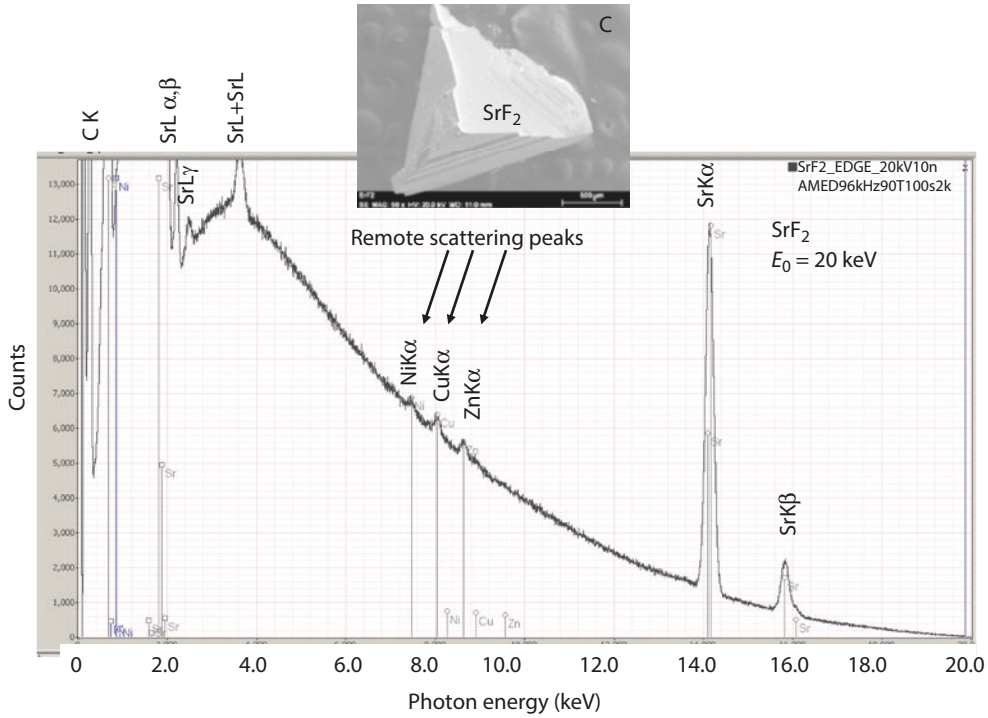

Fig. 21.19 Example with a pyramid of high purity SrF_2 as the scattering target surrounded by a carbon tab (1 cm diameter) on a 2.5 cm diameter brass (Cu and Zn) disk. The Ni signal that is observed likely arises from the Ni-coatings of the specimen stage components

21.5 Summary

High count EDS spectra can be used to achieve limits of detection approaching a mass concentration of $C_{DL} = 0.0001$ (100 ppm) when there are no peak interferences from higher concentration constituents, and $C_{DL} = 0.0005$ (500 ppm) when significant peak interference does occur. However, the analyst must carefully test the SEM/EDS measurement environment to ensure that the trace measurement is meaningful and not a consequence of pathological remote scattering effects.

References

Currie LA (1968) Limits for qualitative detection and quantitative determination. Anal Chem 40:586–593

Newbury DE, Ritchie NWM (2016) Measurement of trace constituents by electron-excited X-ray microanalysis with energy dispersive spectrometry. Micros Microanal 22(3):520–535

Williams DB, Goldstein JI (1981) Artifacts encountered in energy dispersive X-ray spectrometry in the analytical electron microscope. In: Heinrich KFJ, Newbury DE, Myklebust RL, Fiori CE (eds) Energy dispersive X-ray spectrometry, National Bureau of Standards Special Publication 604 (U.S. Department of Commerce, Washington, DC), pp 341–349